Neutron Irradiated Reactor Internals: An Applied Methodology for Specimen Preparation and Post Irradiation Examination by Electron Microscopy Methods

Petra Bublíková[1,2], Patricie Halodová[1], Miroslav Fokt[3], Hygreeva Kiran Namburi[1], Vít Rosnecký[1], Jan Procházka[1], Jan Duchoň[1], Dalibor Vojtěch[2]
[1]Research Centre Řež, Hlavní 130, Husinec – Řež, 250 68. Czech Republic. E-mail: petra.bublikova@cvrez.cz, patricie.halodova@cvrez.cz, hygreeva.namburi@cvrez.cz, vit.rosnecky@cvrez.cz, jan.prochazka@cvrez.cz, jan.duchon@cvrez.cz.
[2]University of Chemistry and Technology Prague, Technická 5, Praha 6 – Dejvice, 166 28, Czech Republic. Dalibor.Vojtech@vscht.cz
[3]Czech Technical University in Prague, Jugoslávských partyzánů 1580/3, Praha 6 – Dejvice, 160 00, Czech Republic. fokt.mirek@gmail.com.

Radiation-induced microstructural defects cause degradation of mechanical properties and a life time reduction of reactor structural components during nuclear power plant operation. The effect of neutron irradiation fluence and flux, neutron spectrum, corrosion environment, etc. on mechanical properties is investigated under the NPP's surveillance programs and additional nuclear material research. The material strength typically increases while ductility and fracture toughness decrease after neutron irradiation. Transmission Electron Microscopy is one of the methods for Post Irradiation Examination (PIE) which helps to understand the material behaviour exposed to different reactor operating conditions. Therefore, such PIE methods are important to develope and optimize. In this study, we introduce the specimen preparation methodology and radiation-induced damage (RID) evaluation of stainless steel SSRT test specimens by the means of Scanning and Transmission Electron Microscopy (SEM, TEM). In austenitic microstructure, Frank interstitial dislocation loops, cavities or voids and radiation-induced precipitates are the dominant RID evolved under neutron irradiation. Futhermore, the material susceptibility to segregation related to the IASCC mechanism is widely studied within 300-series stainless steels. The proper determination of RID size distribution refers to degradation mechanisms in reactor materials. In our research, the RID characterization is demonstrated on the specimens irradiated to ~ 15 dpa in PWR conditions. Distribution of cavities, Frank loops and radiation-induced precipitates were evaluated in bright/dark field kinematical conditions and through-focal series. The nature of cavities, i. e. voids/He or H stabilized bubbles with the size less than 3 nm, was not recognized in the specimens prepared by standard electrolytic polishing method. Radiation-induced segregation in a narrow area up to 10 nm was detected by point STEM-EDS analysis. To evaluate RID size distribution, the automatic image-processing program was developed and compared to the visual analysis. So far, the results were optimized on Frank loops and precipitates and are in a good agreement with the manual processing.

Keywords: Neutron irradiation, PWR, austenitic stainless steels, radiation-induced damage, Transmission Electron Microscopy.

1 Introduction

Mechanical testing of neutron irradiated structural materials is the key information for monitoring of material degradation. The surveillance specimens fabricated from the same alloy as the reactor pressure vessel (RPV) are present inside the active zone and removed periodically during the reactor shutdown for Post Irradiation Examination (PIE). To understand the relationship between mechanical properties – microstructure (microchemistry) changes after neutron irradiation, the raditioninduced damage (RID) is investigated by microscopy techniques to identify even nano-structural defects. Related to the mechanical properties and fracture surface being analysed afterwards, the precise microstructure characterization can help to understand the degradation mechanisms. Microstructural changes due to the neutron irradiation vary with the material composition, irradiation temperature, neutron flux & fluence and energy spectrum [5]. Neutron irradiation can produce a damage by displacing atoms from their lattice positions, which creates point defects such as vacancies and interstitials. Particularly high-energy fast neutron spectrum causing elastic scattering is responsible for such point defects [1]. Most of these defects are annihilated by recombination [1], some of them stay in the microstructure. The vacancies clumping to the clusters (voids) at operating temperature, can be stabilized by transmutation products from nuclear reaction with low-energy neutrons, dependent on the alloying elements. Thereby these products (gases) accelerate the onset of voids swelling, which is the most important contributor to dimensional changes [2]. In the stainless steels (SSs), the He/and or H [3] coming from the reactions with Ni or collant dissolution, diffuse and stabilize the vacancy clusters to form so-called gas-stabilized bubbles [2]. Frank faulted dislocation loops lying on the {111} lattice planes with Burgers vector 1/3 [111], is the another RID observed in the irradiated austenitic microstructure [4]. The loop size increases and loop density decreases with irradiation temperature [5]. From the literature review, at the LWR operating temperature (i. e. around 320°C), the loop density saturates at about 1 dpa and the average loop diameter saturates at 5 dpa [5]. The

austenitic microstructure contains the stable precipitates, i. e. metal particles from the manufacturing process, as well as radiation-induced precipitates (RIP). The γ' (Ni_3Si) and G phase ($M_6Ni_{16}Si_7$) are often formed in 300-series SSs. The migration of vacancies and self-interstitial atoms to the sinks as grain boundaries, dislocations, or precipitate surfaces leads to local chemical changes [12]. The elements such as Si, P, and Ni that are believed to migrate by interstitial mechanisms and enriched near regions that act as sinks for the point defects (e.g. grain boundaries), while elements such as Cr, Mo, and Fe that exchange more rapidly with vacancies are depleted at these sinks. This behaviour is called as Kirkendall mechanism [13]. The significant segregation is observed at irradiation dose of 0.1 dpa, and the effect either saturates or changes very slowly at around 5 dpa [5]. Point defect clusters and precipitates act as obstacles to a dislocation motion that leads to matrix strengthening, resulting in an increase in tensile strength and a reduction in ductility and fracture toughness of the material. The yield strength of irradiated SSs can increase up to five times that of the non-irradiated material after a neutron dose of about 5 dpa. In general, cavities are strong barriers, large faulted Frank loops are intermediate barriers, and small loops and bubbles are weak barriers to dislocation motion [5], depending on their distribution/orientation to the dislocation slip. For the RID determination, PIE methods have been developed and are still optimized. For the nano-scale defect feature characterization, the one of the high-resolution methods is Transmission Electron Microscopy (TEM). To determine microstructural changes under the different irradiation conditions, the density and size distribution are the key parameters. It is important to use a several complementary methods. RID density obtained from TEM micrographs is a feasible, but time-consuming method, as seen from this study. The appropriate complementary method could be Positron Anihilation Spectrocopy (PAS) [6], which can characterize the density of various defects, even to quantify the He-stabilized bubbles [8].

2 Experimental

The experimental material is 15% cold-worked 316 SS. The fabricated SSRT specimens were irradiated to ~ 15 dpa in PWR conditions, i. e. in the mixed spectrum with fast and thermal neutrons at the temperature ~ 320°C. The helium production rate was between 40 and 70 appm/dpa. The mechanical testing was performed in the autoclave in simulated PWR primary water conditions after neutron irradiation. The SSRT was done at the strain rate 5×10^{-8} s^{-1} to investigate the susceptibility to Irradiation Assisted Corrosion Cracking (IASCC). Scanning Electron Microscopy (SEM) micrographs described the intergranular and transgranular brittle/ductile fracture. The material susceptibility to the IASCC can be considered from the dominant intergranular brittle fracture, almost 37%, as seen in *Fig. 1*. Deformation bands associated with the localized deformation were observed at grain boundary facets [4]. The yield strength of irradiated CW 316 specimens was almost 300 MPa higher then reference (non-irradiated) material, total elongation was reduced up to 1.4 % after irradiation.

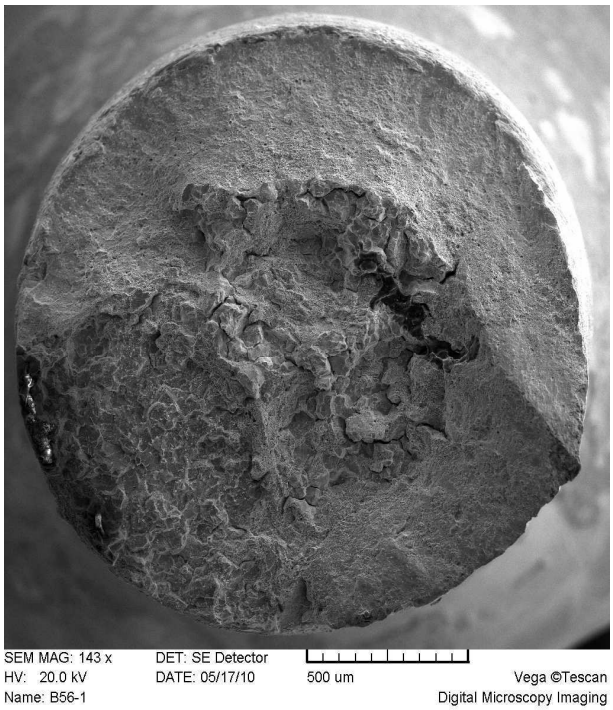

Fig. 1 *SEM micrographs with dominant intergranular brittle fracture [4].*

To attain transparent TEM foils, the optimized methodology was used, based on previous practical knowledge from preparation of 1 mm specimens from ~ 2 mm deformed part of SSRT [7]. The SSRT specimens were cut by diamond saw to the ~300 μm thickness in shielded hot-cells, grinded in glove-boxes to the ~60 μm thickness, then two discs with a diameter of 1 mm were punched from the grinded thin slice and finally electrollyticaly polished. Electrolytic polishing requires the following conditions, the temperature about - 27°C, voltage ~ 27 V, 5% perchloric acid in methanol solution.

3 PIE: Radiation-induced defects characterization

High-Resolution TEM JEOL JEM 2200FS with 200 kV electron source and resolution up to 0.2 nm was used for RID examination, equipped with EDS and energy filter. Cavity population was confirmed on over and under-focused bright-field micrographs. Their size was measured from the intensity profiles across the cavity from the centre of Fresnel fringes (***Fig. 3***). Only the microstructural objects showing the clear change of the contrast indicated inherently presented cavities, have been considered. The cavity density was evaluated by manual processing, i. e. from the overlapping of over and under-focused micrographs (***Fig. 4***). Currently, only the manual image-processing has been applied.

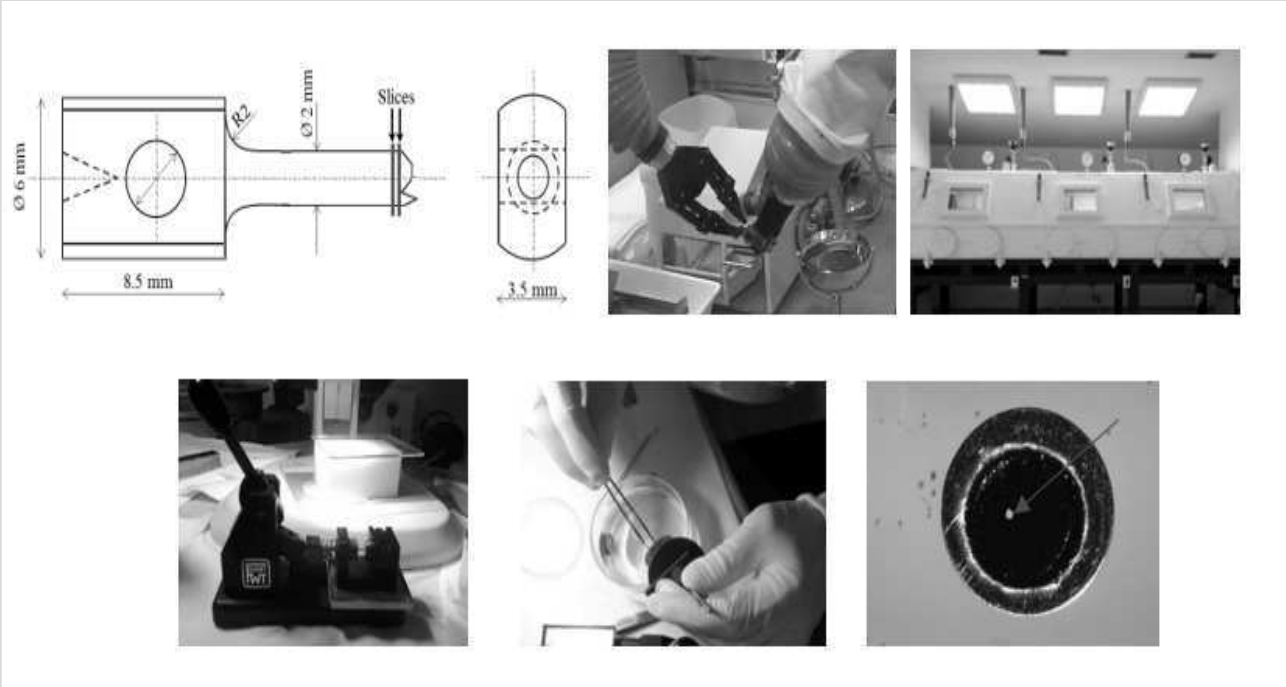

Fig. 2 *The step by step methodology for 1 mm TEM foils preparation from the deformed part of SSRT specimen.*

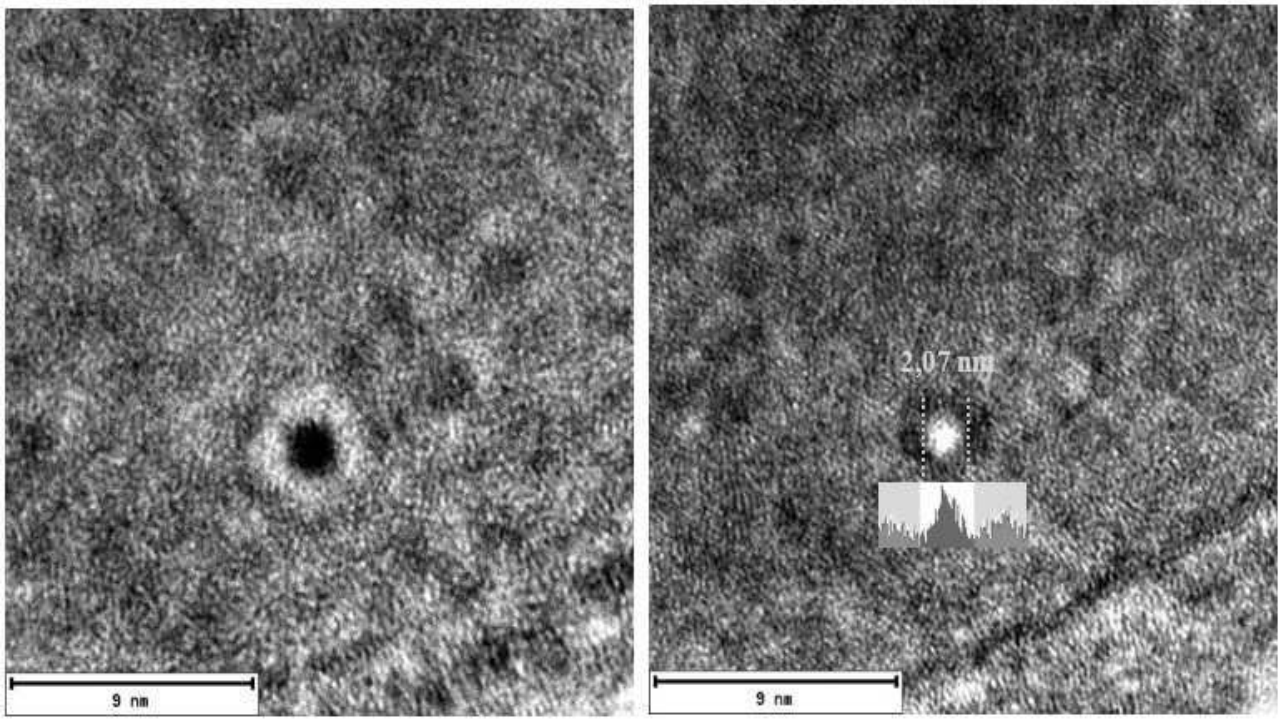

Fig. 3 *Measuring of cavity size from intensity profile of under-focused TEM micrograph (right image).*

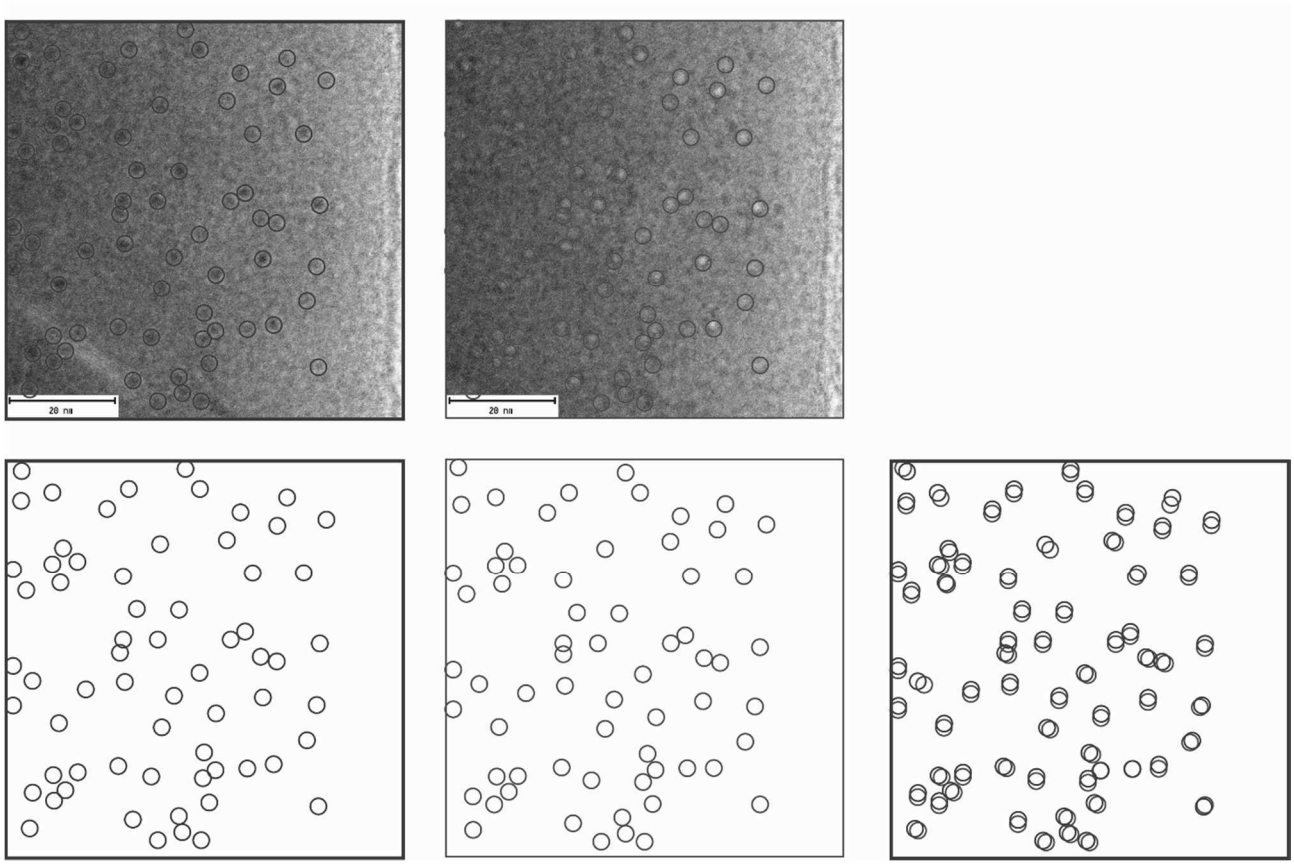

Fig. 4 *Cavities presence confirmed from over (blue) and under (red) - focused TEM micrographs for density evaluation.*

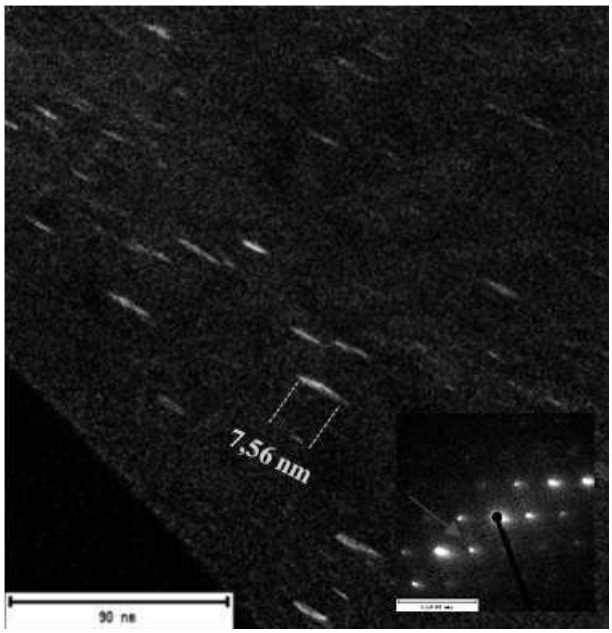

Fig. 5 *Frank loops size determination from dark-field image, corresponding diffraction spot is marked by red arrow.*

Frank loops (FL) and radiation-induced precipitates (RIP) were imaged in dark-field (DF) conditions using the corresponding diffraction spots (***Fig. 5, 6***). The average RIP diameter was calculated from the micrographs taken at higher magnification, FL size was calculated from rel-rod DF. To refine the RID size distribution and optimize the time-consuming manual processing, the new program was developed and firstly applied on FL and RIP imaged in dark-field [9]. The script written in the program MatLab is based on automatic detection of the bright features (FL, RIP) with defined intensity. The slight image pre-processing for the noise reduction had to be applied on the micrographs (***Fig. 6***). The script details are described by the author M. Fokt in [9].

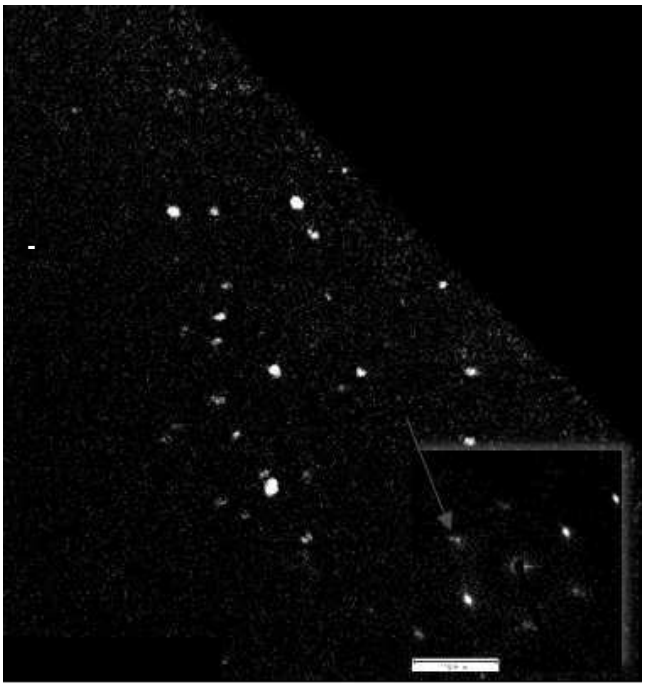

Fig. 6 *Radiation-induced precipitates imaged in dark-field conditions with corresponding diffraction spot marked by red arrow. Noise reduction for the automatic image-processing [9].*

4 Results and discussion

Cavity presence evaluated manually from the overlapping of over and under-focused TEM micrographs confirmed the uniform distribution in the 316-deformed microstructure (*Fig. 7*). More than 600 cavities were evaluated. The volume density was calculated [10] in the order of magnitude $10^{22} \pm 10^{21}$ m^{-3} with the average cavity size 2.0 ± 0.8 nm (almost all cavities were 1-2 nm in diameter). The results are comparable to the previous research on the same material [4]. The cavity size is very small to decipher the cavity nature (vacancy voids/He bubbles). The transparent area after electrolytic polishing is not thin enought to resolve the gas-stabilized bubbles in the austenitic matrix in STEM-HAADF micrographs and the specimen was not suitable for further EELS analysis. In the microstructure, there were not observed any cavity denuded zones, only the uniformly distributed cavity population. The cavity presence likely contributes to the increasing of yield strength, ultimate tensile strength and reducing the ductility known from SSRT experiment. Cavity population obviously helps to the radiation hardening, which may lead to the brittle fracture mechanism [17].

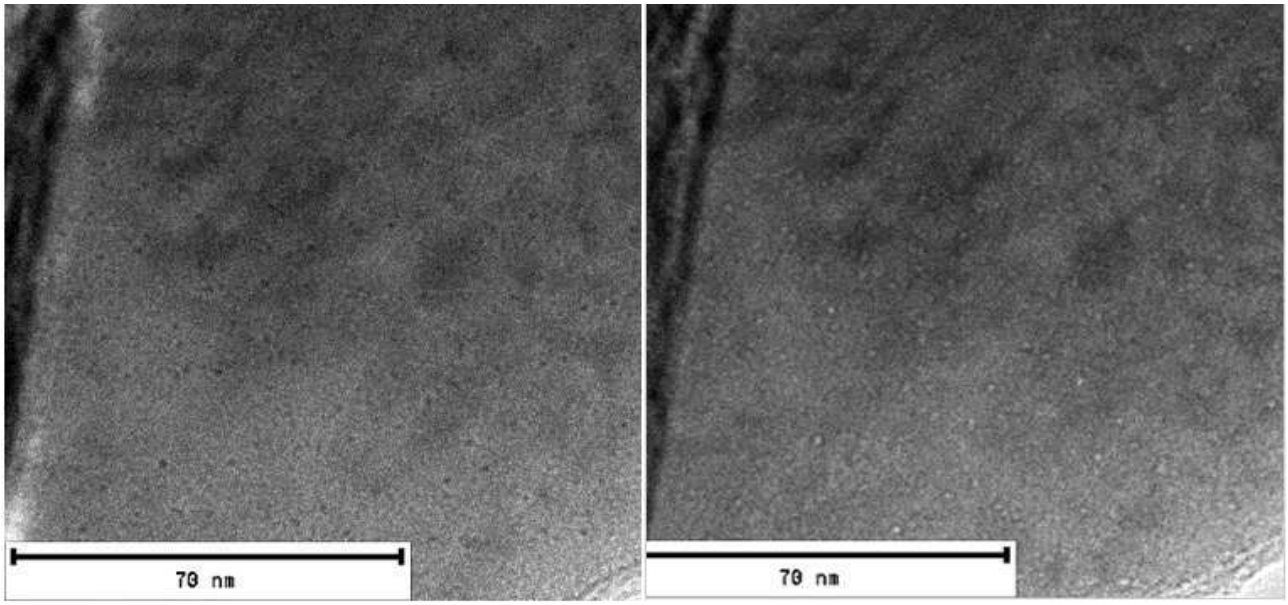

Fig. 7 *Uniformly distributed cavity population in the austenitic microstructure in over and under-focused micrographs.*

Frank faulted dislocation loops, with Burgers vector 1/3 [111] lying on the {111} planes, were imaged under rel-rod dark-field conditions near the matrix zone axis z = [011]. The manual evaluation of FL density is in a good agreement with the program processing, i. e. the FL density was calculated in the same order of magnitude 10^{22} m^{-3} from about ten micrographs. The FL size was evaluated higher with the higher standard deviation by the program processing, as seen in *Table 1*. It can be probably caused by higher resolution of the bright areas determined by program compared to a human eye. The FL size distribution obtained by program and "by hand" is in the *Graph 1*. The results from FL studies are similar with the previous research on irradiated cold-worked 316 SS [4]. Futhermore the results also confirm the saturation of FL at 5 dpa [4], [5]. Evaluation of RIP density show the comparable results from manual and automatic image-processing as for the Frank loops, seen in *Table 1*. The size distribution shows the difference in size evaluated "by hand" and by program, *Graph 2*. It can be caused by pre-processing of the micrographs which can enlarge the RIP diameter. However, both methods for RID evaluation imaged in dark-field show the uniform distribution in the matrix. Frank loops as well as RIP likely contribute to the material strengthening and hardening at the expense of the ductility together with the evaluated cavity population.

Tab. 1 *Frank loops and RIP evaluated manually "by hand" and automatically "by program" [9].*

RID	Evaluation method	Average size *d* (nm)	Volume density N_v (m^{-3})
Frank loops	by program	12.6 ± 6.6	2.1 ± 0.8 x 10^{22}
	by hand	6.6 ± 3.7	2.1 ± 1.6 x 10^{22}
Radiation-induced precipitates	by program	4.2 ± 2.0	6.0 ± 1.6 x 10^{21}
	by hand	4.5 ± 1.1	5.9 ± 1.1 x 10^{21}

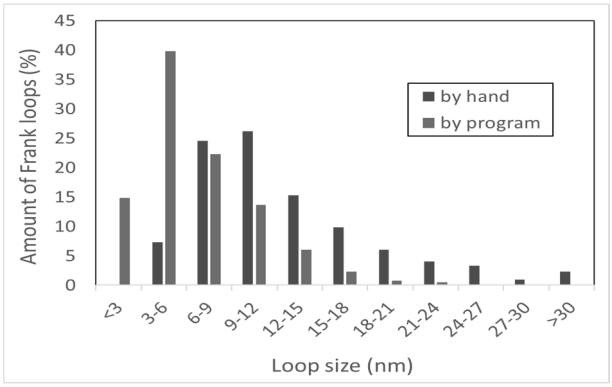

Graph 1 *Frank loop size distribution evaluated manually "by hand" and by program processing [9].*

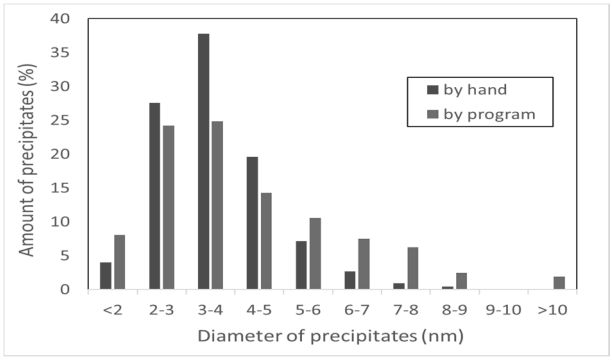

Graph 2 *Size distribution of radiation-induced precipitates (RIP) evaluated "by hand" and by program processing [9].*

Another effect of radiation on microstructure which likely contributes to IASCC is Cr-depletion by vacancy mechanism leading to decreased grain boundary corrosion resistance [17]. Then the localized deformation on grain boundaries affected by Cr-depletion and corrosion environment can cause the crack initiation [14]. Si, P, or Ni elements, which migrate by interstitial mechanism, enrich near grain boundary regions [18]. The extent of segregation/depletion (S/D) at grain boundaries is decreased, and the width of the profile is increased with the temperature increase. The grain boundary S/D profiles are extremely narrow at about 300°C [5]. Cr&Fe depletion and Si&Ni enrichment at high-angle grain boundaries up to 10 nm width, was observed in the experimental material using STEM-EDS point spectrum (*Graph 3*) [15]. Depending on the material and irradiation conditions, the concentration changes may be significant, as presented in reviews [14], [16]. Futhermore, Cr promotes the formation of W-shape changing with the dose level to V-shape [18], for cold-worked 316 SS the change is reported from 6 dpa [5]. In the experimental material, the V-shape with Fe&Cr depletion was observed.

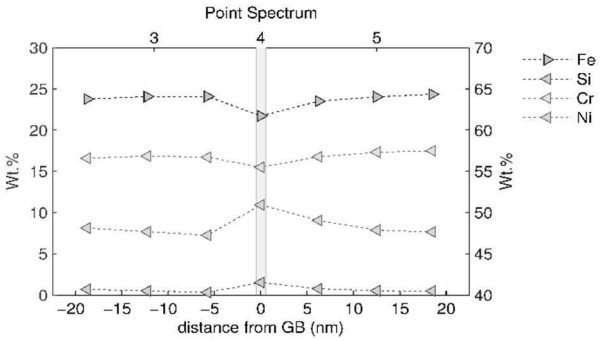

Graph 3 *Cr&Fe depletion and Ni&Si enrichment at high-angle grain boundary [15].*

One of the effect of evaluated RID on a microstructure, which have been hypothesized to IASCC contribution, is the matrix hardening leading to weakening of grain boundaries relative to the matrix [17]. Support for the matrix hardening contribution was provided by Was and Bruemmer who showed that intergranular SCC susceptibility correlated reasonably well with increasing yield stress [11]. As well, the explanation is presented by the change in deformation mode caused by irradiated microstructure and the interaction of localized deformation bands with grain boundaries [17]. Futhermore, the Cr-depletion can significantly decrease the corrosion resistance. Different approaches to the IASCC explanation are still being investigated since the phenomenon has occurred. Further studies to clarify the mechanism are still required [16].

5 Conclusions

The SSRT specimens of cold-worked 316 stainless steel after the irradiation to ~15 dpa in LWR conditions were investigated by Transmission Electron Microscopy. The radiation-induced damage was characterized by manual as well as automatic image-processing. The new program was developed to reduce the time-consuming manual evaluation and to optimize the results. For the study, the transparent 1 mm TEM foils were prepared from the deformed part of SSRT specimens.

Currently, the program processing was optimized for Frank loops and radiation-induced precipitates imaged in dark-field conditions. The results from program processing are in a good agreement with the manual evaluation, i. e. the density of FL and RIP was calculated in the same order of magnitude 10^{22}, 10^{21} respectively. Cavity population was distributed uniformly in the 316-deformed microstructure, the density was in the order of magnitude $10^{22} \pm 10^{21}$ m^{-3} with the average cavity size 2,0 ± 0,8 nm. Such small dimensions did not allow to recognize the cavity nature in the specimens prepared by classical electrolytic polishing. Currently, the cavity size distribution was

calculated manually. The size distribution of Frank loops and cavities is in a good agreement with the results obtained on the same material.

The local microstructural/chemical changes have been investigated. Cr&Fe depletion and Si&Ni enrichment was revealed at the high-angle grain boundaries, Cr&Fe depletion was observed in V-shape.

RID observed in the microstructure are likely responsible for the mechanical properties changes, i. e. increasing of yield strength, ultimate tensile strength and reducing the ductility known from SSRT experiment. Dense population of radiation-induced defects together with local changes as the Cr-depletion likely contributes to IASCC mechanism.

Acknowledgement

The presented work was financially supported by the Ministry of Education, Youth and Sport Czech Republic (National Programme of Sustainability II) Project LQ1603 (Research for SUSEN).

References

[1] HOJNÁ, A. (2016). Open questions related to the material parameters of the reactor internals at assessing the operating time, In: *Nuclear safety* 24 (62).

[2] GARNER F.A. (2012). Radiation Damage in Austenitic Steels. Comprehensive Nuclear Materials. In: *Elsevier,* Vol. 4, p. 33-39.

[3] HOJNÁ, A., NAMBURI, H., DUCHOŇ, J., HALODOVÁ, P. (2018). Effect of strain rate and high temperature water on deformatioin structure of VVER neutron irradiated core internals steel. *Proceedings of the 18th International Conference on Environmental Conference on Environmental Degradation of Materials in Nuclear Power Systems – Water Reactors.* ISBN 978-3-319-67244-1.

[4] ERNESTOVÁ, M., BURDA, J., KOČÍK, J., MICHALIČKA, J., POKOR, C. (2014). Influence of the neutron spectrum on the sensitivity to IASCC and microstructure of CW 316 material. *Contribution of Materials Investigation and Operating Experience to LWRs Safety, Performance and Reliability.*

[5] CHOPRA, O. K. (2010). Degradation of LWR core Internal Materials due to Neutron Irradiation. NUREG/CR-7027.

[6] KOČÍK, J., KEILOVÁ, E., ČÍŽEK, J., PROCHÁZKA, I. (2002). TEM and PAS study on neutron irradiated VVER-type RPV steels. *Journal of Nuclear Materials.* Vol. 303, p. 52 – 64.

[7] NAMBURI, H. K., BUBLÍKOVÁ, P., ROSNECKÝ, V. (2015). TEM Foils Preparation from Irradiated Austenitic Stainless Steel - An applied methodology to attain 1mm samples. *23rd International Conference Nuclear Energy for New Europe.* ISBN 978-961-6207-37-9.

[8] XU, Q., POPOV, V., TROEV, T., ZHANG, J., DAI, Y. (2018). Positron lifetime calculation of vacancy clusters in tantalum containing hydrogen and helium. *Journal of Nuclear Materials.* Vol. 506, p. 71 – 75.

[9] FOKT, M. (2018). Signal analysis of transmission electron microscopy observations of bubbles and defect clusters in austenitic steels irradiated in a nuclear reactor. Thesis (Ing.). Czech Technical University in Prague, Faculty of Nuclear Science and physical engineering. 2018-05-07.

[10] EGERTON, R. F. (2011). Electron Energy-Loss Spectroscopy in the Electron Microscope, *Springer*, London.

[11] WAS, G.S., BRUEMER, S. M. (1994). *J. Nucl. Mater.,* 216, 326.

[12] ALLEN, J. I., WAS, G. S., KENIK, E. A. (2002) Radiation-induced segregation and the relationship to physical properties in irradiated austenitic alloys. In: *National Society of Black Physicists Conference Procedings.*

[13] FUKUYA, K. (2013). Current understanding of radiation-induced degradation in light water reactor structural materials. In: *Journal of Nuclear Science and Technology*. 50:3, 213-254, DOI: 10.1080/00223131.2013.772448.

[14] HOJNÁ, A. (2013). Irradiation Assisted Stress Corrosion Cracking and Impact on Life Extension. *Corrosion*. Available from: http://corrosionjournal.org/doi/abs/10.5006/0803. ISSN 0010-9312.

[15] BUBLÍKOVÁ, P., HALODOVÁ, P., DUCHOŇ, J., LIBERA, O., NAMBURI, H. K., ERNESTOVÁ, M., STODOLNA, J. (2018). TEM examinations of radiation-induced damage and nanoindentation on CW 316 steel irradiated in different neutron spectra. *Fontevraud 9 - Int. Symposium on Contribution of Materials Investigations and Operating Experience to Light Water NPPs' Safety, Performance and Reliability.*

[16] HOJNÁ, A. (2017). Overview of Intergranular Fracture of Neutron Irradiated Austenitic Stainless Steels. *Metals*. 7, 392.

[17] WAS, G. S., BUSBY, J. T. (2005). Role of irradiated microstructure and microchemistry in irradiation-assisted stress corrosion cracking. *Philosophical Magazine*, 85:4-7, p. 443-465, DOI: 10.1080/02678370412331320224.

[18] KENIK, E. A., BUSBY, J. T. (2012). Radiation-induced degradation of stainless steel light water reactor internals. Materials Science and Engineering R. 73, p. 67 – 83.

10.21062/ujep/135.2018/a/1213-2489/MT/18/4/545